Experimental study of attenuation and dispersion over a broad frequency range: 2. The universal scaling of polycrystalline materials

Christine McCarthy,[1] Yasuko Takei,[1] and Takehiko Hiraga[1]

Received 25 March 2011; revised 14 June 2011; accepted 20 June 2011; published 27 September 2011.

[1] In order to extend the range of conditions that can be obtained in experiments, we have measured the viscoelastic properties of polycrystalline organic borneol, as an analogue to mantle rock. Using a custom fabricated apparatus, the Young's modulus E and attenuation Q_E^{-1} were measured accurately over a broad frequency range ($10^{-4} \leq f$ (Hz) $\leq$ 2.15) and at low strain amplitude (10^{-5}–10^{-6}). Creep experiments were performed with the same apparatus to measure the steady state viscosity. Anelasticity and viscosity were measured at high homologous temperatures (T = 22–48°C; T/T_m = 0.61–0.67) and various grain sizes (3–22 μm), the growth of which was controlled by annealing. Using the measured viscosities η and the unrelaxed modulus E_U determined from ultrasonic experiments, the frequency of the entire data set was normalized by the Maxwell frequency $f_M = E_U/\eta$, resulting in E and Q^{-1} master curves. The Q^{-1} data from previous studies on olivine-dominated samples also collapse onto the same curve when scaled by f_M, demonstrating the universality of anelasticity for polycrystalline materials. The similitude by the Maxwell frequency scaling indicates that the dominant mechanism for the anelasticity observed in this study and in previous studies is diffusionally accommodated grain boundary sliding. A generalized formulation for this similitude is provided to extrapolate the experimental data to velocity and attenuation of seismic shear waves.

Citation: McCarthy, C., Y. Takei, and T. Hiraga (2011), Experimental study of attenuation and dispersion over a broad frequency range: 2. The universal scaling of polycrystalline materials, *J. Geophys. Res.*, *116*, B09207, doi:10.1029/2011JB008384.

1. Introduction

[2] In the past, the elastic properties of rocks at high temperatures and pressures have been measured using ultrasonic techniques or Brillouin scattering methods and, hence, have been limited to high frequencies (MHz-GHz) [e.g., *Isaak*, 1992; *Jacobsen et al.*, 2008]. Because seismic waves have much lower frequencies (10–10^{-4} Hz), the frequency dependence (or dispersion) of elastic wave velocities is an important issue to be clarified. Velocity dispersion and associated attenuation are collectively referred to as "anelasticity" [e.g., *Anderson*, 1989]. For a one-dimensional seismological structure, such as PREM [*Dziewonski and Anderson*, 1981], experimentally measured wave velocities agree well with seismologically measured velocities, and detailed studies on mantle mineralogy have been successfully performed via direct comparison of seismological and high frequency experimental data [e.g., *Duffy and Anderson*, 1989; *Stixrude and Lithgow-Bertelloni*, 2005]. This suggests that velocity reduction by dispersion at seismic frequencies is small enough to interpret one-dimensional seismological structure in the Earth. Therefore, relatively small attention has been paid to rock anelasticity. However, recent progress in seismology has revealed highly resolved, three-dimensional velocity and attenuation structures [e.g., *Nakajima and Hasegawa*, 2003; *Tsumura et al.*, 2000; *Wiens et al.*, 2006]. Because dispersion plays a significant role in causing small perturbations in seismic wave velocity through thermal and/or chemical heterogeneity in the Earth [*Karato*, 1993; *Karato and Jung*, 1998], and also because anelasticity influences attenuation structure, renewed interest in the laboratory study of anelasticity has been prompted.

[3] Experimental studies at seismic and subseismic frequencies have greatly expanded our understanding of rock anelasticity at high homologous temperature [e.g., *Gribb and Cooper*, 1998; *Tan et al.*, 2001; *Jackson et al.*, 2002, 2004; *Sundberg and Cooper*, 2010]. In order to minimize thermal cracking, these studies used natural and synthetic olivine-dominated aggregates with much smaller grain size (d = 3–150 μm) than that of mantle rocks ($d \sim$ 1 mm). Therefore, extrapolation of experimental data to mantle conditions is contingent on our assessment of the appropriate grain size sensitivity of anelasticity. It has been widely known that there exists similitude in anelasticity, such that frequency, temperature, grain size, and pressure dependences can be captured by a single "master variable." Characterization of the master variable is essential to identifying the underlying mechanism of anelasticity and to applying laboratory-

[1]Earthquake Research Institute, University of Tokyo, Tokyo, Japan.

0148-0227/11/2011JB008384

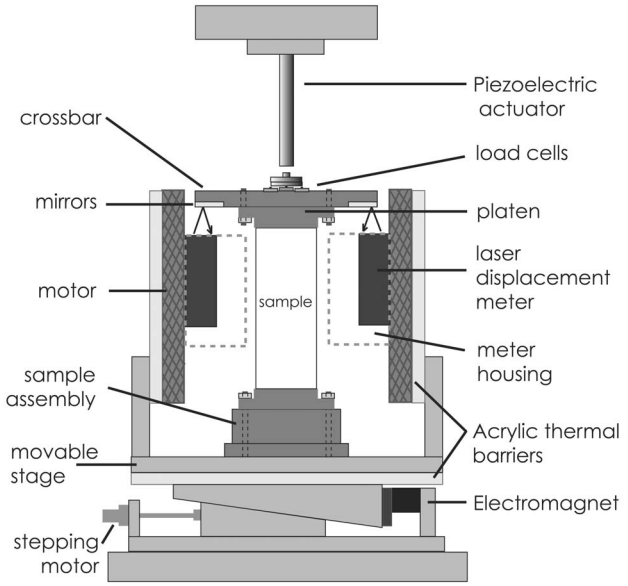

Figure 1. Schematic of the custom-fabricated, cyclic compressive, forced-oscillation apparatus. During testing, the whole apparatus rests in a temperature-controlled incubator.

derived insights to seismology. However, a consensus among researchers has not yet been reached about this issue. *Gribb and Cooper* [1998] first proposed the idea of similitude based on the classic model of anelasticity by diffusionally accommodated grain boundary sliding [*Raj and Ashby*, 1971; *Raj*, 1975]. They suggested that the master variable is normalized frequency, that is, frequency scaled by the Maxwell relaxation frequency defined by diffusion creep viscosity. *Jackson et al.* [2002] demonstrated the similitude with the attenuation spectra measured for various grain sizes and temperatures. Although many of their observations are consistent with predictions from the model of diffusionally accommodated grain boundary sliding, the master variable obtained from their data exhibited a different grain size dependence than what is expected from this mechanism. Recently, *Morris and Jackson* [2009a] extended the test of similitude by examining multiple data sets on olivine-dominated samples from several laboratories and applying the Maxwell frequency scaling. However, due to a lack of viscosity measurements for some of the studies, the estimated Maxwell frequencies were subject to large uncertainty.

[4] As discussed above, a detailed analysis of anelasticity requires accurate and reliable measurement of elasticity and viscosity. However, anelasticity data with reliable viscosity data measured under known creep mechanisms are still lacking. In this study, we use an organic polycrystalline material as an analogue to mantle rock to accurately measure anelasticity and viscosity at various grain sizes and temperatures. This organic material has been shown to be an appropriate analogue to earth materials and detailed measurements of its elasticity have previously been performed [*Takei*, 2000]. In the companion paper, we discuss a new apparatus for measuring attenuation and Young's modulus with great precision over a broad range of frequencies. Here we report experimental data from a suite of experiments performed within this apparatus. Detailed analyses of the data, including a test of the similarity principle and extrapolation to seismic frequencies, are reported.

2. Experimental Details

2.1. Sample Fabrication

[5] Polycrystalline samples were created using borneol ($C_{10}H_{18}O$; T_m = 204.5°C), which is classified as a plastically crystalline organic that deforms by the same kinds of dislocation and diffusion processes as minerals, metals and ceramics [*Sherwood*, 1979]. Very fine borneol powder (~3 μm) obtained from a cold ball-milling procedure (−40°C, 6 days) was placed in a cylindrical die and pressed to 13.9 MPa at ambient temperature for ~48 h to produce fully dense, polycrystalline right circular cylinders (height = 60–70 mm; diameter = 30 mm). A Teflon inner sleeve allowed removal of the sample from the die without fracture. This method resulted in translucent (i.e., nonporous) samples with very uniform and fine initial grain size (~3 μm). After attaching two end platens, the sample and platens were sealed in a nonreactive plastic bag to prevent sublimation during mechanical testing and annealing. A mirrored crossbar and steel base plate were clamped tightly to the platens. We will refer to these components together as the "sample assembly" (Figure 1). The sample assembly is described in greater detail in the companion paper [*Takei et al.*, 2011].

2.2. Mechanical Testing

[6] In order to explore the mechanical properties of the analogue material borneol over the full range of its viscoelastic response (elasticity, anelasticity and viscosity), a variety of tests were employed. In a previous study, the shear and longitudinal wave velocities (V_s and V_p, respectively) were measured in pure borneol samples at ultrasonic frequency ($f \cong 1$ MHz at $18 \le T(°C) \le 60$) [*Takei*, 2000]. From such data, the complete set of elastic constants, including the unrelaxed Young's modulus E_U, was obtained. Because E_U represents the crystal property, it does not depend on grain size but was found to have a temperature dependence of the form: $E_U(T°C) = 2.574$ (GPa) − 0.00334 (GPa/°C) × T(°C). In this study, forced oscillation and creep tests were performed to measure anelasticity and viscosity, respectively.

[7] Young's modulus and attenuation of borneol samples were measured in cyclic compressive loading tests as functions of frequency, using the custom-fabricated apparatus (Figure 1) fully described in the companion paper [*Takei et al.*, 2011]. A piezoelectric actuator applied a series of sinusoidal cycles, in addition to an offset stress, starting with the highest frequency and systematically working to the lowest frequency at logarithmically equally spaced frequencies (three per decade). At $f \ge 0.0464$ Hz about 30 cycles were used in testing; between $0.0464 > f$ (Hz) ≥ 0.00215, about 10 cycles were tested; between $0.00215 > f$ (Hz) ≥ 0.000215 about 5 cycles were tested; and, due to oscilloscope data logging capacity, only 2.4 cycles were tested for $f = 10^{-4}$ Hz. Stress was monitored by load cells and the response of the sample was measured by a pair of laser displacement meters with resolution of 10^{-8} m (with a 60–70 mm sample height, this corresponds to strain resolution of $\sim 10^{-7}$) and with sampling frequencies larger than 500 × f. The offset stress was 0.28 MPa and the amplitude of the

Table 1. Experimental Conditions for This Study

Sample	Grain Size, d[a] (μm)	Temp, T[a] (°C)	Thermal History, (°C) (days)	Corrected Viscosity[b] (Pa s)	Maxwell Relaxation Time[c] (τ_M s)	Accumulated Strain[d]
11	4.8	27.8(±1.5)[e]	Initial	b. 7.22×10^{12}(+0.1)	3004	0.0309
15	3.35(0.15)	23.6(±0.3)	Initial	a. 7.80×10^{12}(+0.1)	937.2	0.0122
				b. 2.04×10^{12} (−1.4)		
15	4.15(0.25)	23(±0.3)	30(1)	a. 2.34×10^{12} (−0.2)	2217.2	0.0254
				b. 5.28×10^{12} (−0.5)		
15	5.06(0.24)	22.7(±0.1)	30(4)	a. 5.81×10^{12} (0)	3390.3	0.0304
				b. 8.66×10^{12} (−0.9)		
15	7.99(0.53)	22.4(±0.2)	30(4);40(0.8)	a. 8.29×10^{12} (−0.2)	6263.6	0.0335
				b. 1.51×10^{13} (−0.4)		
15	8.9(0.82)	22.9(±0.05)	30(4);40(2.8)	a. 1.62×10^{13} (+0.2)	10335	0.0349
				b. 2.63×10^{13} (−0.7)		
15	15.3(0.89)	23(±0.4)	30(4);40(8.8)	a. 2.54×10^{13} (+0.6)	12182	0.0361
				b. 3.05×10^{13}(−0.8)		
15	18.7(1.29)	22.6(±0.3)	30(4);40(8.8);45(5)	a. 4.12×10^{13} (+1.0)	16498	0.0381
15	22.0(0.27)	23.7(±0.2)	30(4);40(8.8);45(5);50(6)	b. 5.09×10^{13} (+0.3)	20332	0.0384
15	22.0(0.27)	31.4(±0.1)	30(4);40(8.8);45(5);50(6)	b. 1.96×10^{13}(−0.1)	7839	0.0401
15	22.0(0.27)	41.4(±0.05)	30(4);40(8.8);45(5);50(6)	b. 6.22×10^{12}(+0.1)	2487	0.0423
15	22.0(0.27)	45.4(±0.1)	30(4);40(8.8);45(5);50(6)	b. 5.10×10^{12}(−0.05)	2039	0.0466
15T[f]	21.4					
16	4.3(0.2)	23.5(±0.3)	Initial	b. 4.09×10^{12} (−1.5)	1654	0.0102
16	6.3(0.1)	23(±0.3)	30(4)	a. 4.18×10^{12} (−0.4)	4250	0.0174
				b. 1.06×10^{13} (−0.3)		
17	21.4(1.6)	22.5(±0.3)	60(14)	b. 5.25×10^{13}(+0.1)	20994	0.0263
17	21.4(1.6)	30.8(±0.05)	60(14)	b. 1.90×10^{13}(−0.1)	7695	0.0277
17	21.4(1.6)	39.4(±0.5)	60(14)	b. 8.01×10^{12}(+0.1)	3284	0.0305
17	21.4(1.6)	47.7(±1)	60(14)	b. 3.37×10^{12}(−0.1)	1399	0.0363
17T	23.8(0.7)					

[a]Values in parentheses are measures of error in μm for grain size and °C for temperature.
[b]Viscosity measured before "b" and after "a" anelasticity testing. In parentheses is temperature in degrees above or below the value of the anelasticity test (in Temp. column).
[c]The average of the before and after viscosities divided by temperature-dependent E_U.
[d]At the onset of anelasticity runs, i.e., the final value of the previous creep test.
[e]The temperature error of Sample 11 is large because this run is performed before improvements made to the apparatus for thermal insulation.
[f]T represents the grain size measurements of testing samples.

sinusoidal stress (zero-to-peak) was 0.055 MPa, which was nearly constant for all testing frequencies. As discussed in the companion paper, the offset stress slightly decreases during a set of cycles as the sample shortens by creep. At the beginning of each new set of cycles, the movable stage (Figure 1) was programmed to rise until the desired offset stress was again obtained. Therefore, at low frequencies, the data acquisition was delayed for a predetermined length of time to omit transient effects associated with the reapplied stress.

[8] Using the same apparatus, viscosity η (Pa s) was measured via creep tests, in which a nominally constant stress ($\sigma = 0.28 \pm 0.01$ MPa) was applied and the shortening of the sample was measured over time. The stress was controlled by adjustments to the height of the movable stage, and sample displacement was measured by the total steps applied to raise the stage and by the displacement meters, both of which gave consistent results. Because the initial stress of each creep test was not always zero and the sampling rate was less than 10^{-2} Hz, creep data were only used to obtain the steady state viscosity and not any transient properties.

[9] The entire apparatus was placed in a temperature-controlled incubator, which was placed on a vibration-free tabletop. The temperature of samples during testing, which was monitored by a thermocouple placed in the top of the movable stage (T_1) and a thermocouple in the air surrounding the sample (T_2), is expressed as $T = (T_1 + T_2)/2 \pm |T_1 - T_2|/2$. As discussed in the companion paper, the temperature distribution inside the incubator represents a playoff between the heating of some apparatus components and the cooling of compressed air circulating through meter housings. However, for each run, airflow was held constant and the temperature of the entire system was allowed to equilibrate for ~8 h (without load), so that temporal temperature deviation during testing was <0.2°C. Spatial deviation $|T_1 - T_2|$ was <0.6°C for all tests, except at the highest temperature, where the deviation was approximately 2°C.

2.3. Experimental Procedures

[10] In Table 1 we summarize the experimental conditions of this study. One notable aspect of our approach is that mechanical tests were made on *the same polycrystalline sample* at various grain sizes ("grain size tests") and temperatures ("temperature tests"). This continuity enabled a detailed investigation of temperature and grain size dependences without any fabrication influences.

2.3.1. Grain Size Tests

[11] Anelasticity and viscosity were measured at approximately constant temperature in the range $T = 22.4$–23.7°C and at various grain sizes from 3.4 μm to 22 μm (Figure 2). A sample without any thermal history ("initial" in Table 1)

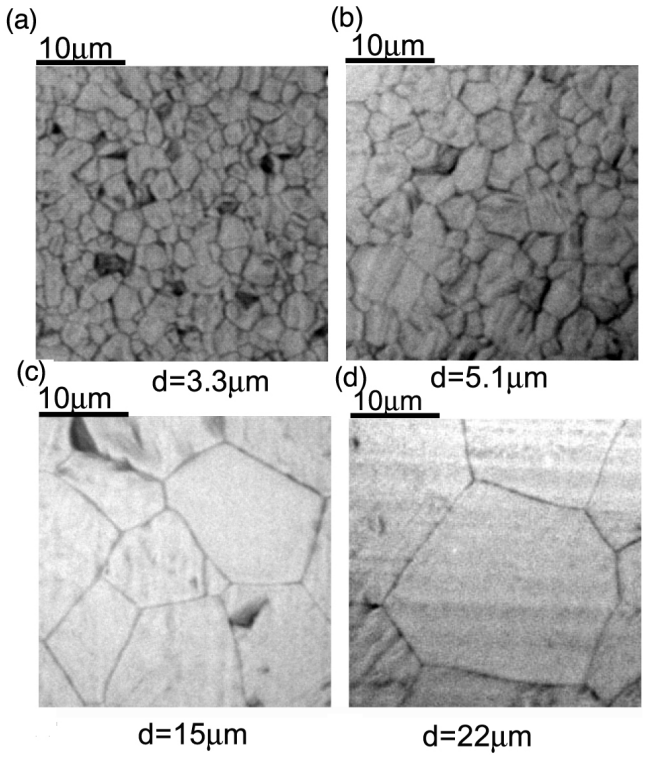

Figure 2. Light microscope images of pure borneol sample (sample 15) with grain sizes of approximately (a) 3 μm (initial), (b) 5 μm, (c) 15 μm, and (d) 22 μm. The sample shown in Figures 2b–2d experienced controlled grain growth via high-temperature annealing.

was loaded into the sample assembly and tightly fixed to the apparatus, a uniaxial stress (0.28 ± 0.01 MPa) was applied, and the sample deformed for one or two days under nominally constant stress to ensure good contact with the two end platens. In this temperature range, grain growth is negligible even for the smallest grain size samples. After measuring anelasticity and viscosity at the initial grain size, the sample was isothermally annealed at temperatures between 30°C and 60°C for various durations within a temperature-controlled incubator. During the anneal, the sample remained fixed in the sample assembly, but all compressional load was removed. Uniaxial creep tests were conducted both before and after each series of forced oscillation tests, allowing us to confirm that no undesired change in viscosity (due to evolution of grain size or defect structure) had occurred during the course of the run.

[12] Grain size was measured by employing a miniature companion sample (diameter = 15 mm; length ≈ 15 mm) that was created with the same starting powder and at the same conditions as the testing sample. This miniature sample shadowed the testing sample at all times and was used to periodically monitor grain size evolution without destruction of the testing sample. Confirmation of the approach was made via comparison of the final grain size of the testing sample to that of its miniature. For each grain size analysis, one face of the miniature sample was polished to a mirror finish with a microtome and examined with a high-resolution, real color confocal microscope (Lasertec Optelics C130). Slight sublimation at grain boundaries at ambient pressure and temperature obviated the need for etching (Figure 2). Images containing no fewer than 100 grains were analyzed to measure mean grain size using the line intercept method with a correction factor of 1.5 [*Gifkins*, 1970]. Two researchers analyzed each specimen in at least two positions each and the values obtained were averaged. The grain size error listed in Table 1 constitutes the deviation from this mean.

2.3.2. Temperature Tests

[13] After the grain size tests were completed, coarse-grained samples were used to measure anelasticity and viscosity at constant grain size (d = 22 μm) and at various temperatures from 22 to 48°C, which represent homologous temperatures $0.61 < T/T_m < 0.68$. Considering the relatively long anneal times and elevated temperatures used for grain growth during the grain size testing stage, grain growth during the temperature tests was predicted to be negligibly small. That results from temperature tests pertain to constant microstructure was confirmed by the reproducibility of anelasticity and viscosity once the specimen was returned to low temperature, as well as by microstructural analysis of the miniature and testing samples once the temperature tests were completed.

2.3.3. Linearity Tests

[14] To ensure the linearity of our data, tests were performed on a fine grain sample to determine Young's modulus and attenuation as functions of stress/strain amplitude. A series of sinusoidal cycles at decreasing frequencies, with only one oscillation frequency per decade, was applied to a sample (in addition to the constant offset stress) at T = 27.8°C. The series was repeated for a total of four different stress/strain amplitudes, in random order.

2.4. Data Analysis

[15] Several formulae used in this section assume linearity of the samples, which was confirmed in the experiments.

2.4.1. Forced Oscillation Tests

[16] Typical raw experimental data are shown in Figure 3. The monotonic upward trend of the strain data (contraction positive) is steady state creep associated with the offset

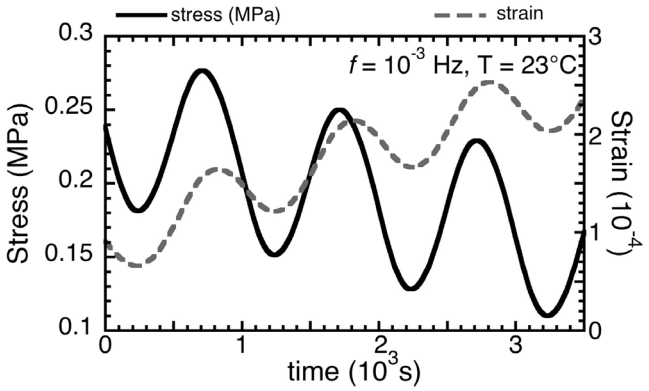

Figure 3. Typical raw data of stress and strain for borneol aggregates at $f = 10^{-3}$ Hz and T = 23°C (compression and contraction positive). The linear trend of the strain data shows creep in the sample due to the offset stress. The linear trend of the stress curve shows the gradual relaxation of the offset stress due to the sample creep.

stress and the monotonic downward trend of the stress data (compression positive) is the relaxation of the offset stress due to such creep. These linear trends were removed from the data by determining the slope during each cycle based on the change in value of a specific point in adjacent cycles. With this method, any variation of slope from one cycle to the next can be taken into account. However, this method cannot be used when the slope changes within one cycle, as is often the case in early cycles of very low frequency testing ($<10^{-3}$ Hz) of samples with small grain size or at high temperatures (i.e., conditions in which the sample is very soft). In such cases, these cycles were removed from the analysis. At the lowest frequency (10^{-4} Hz), removal of any portion of the already short data set (only 2.4 cycles) can affect the experimental results. The error associated with this procedure is discussed in more detail in section 3.1.

[17] Once the linear trends are removed from the data, stress and strain can be expressed as

$$\sigma(t) = \sigma_0 \cos(\omega t - \Phi_\sigma) \tag{1}$$

$$\varepsilon(t) = \varepsilon_0 \cos(\omega t - \Phi_\varepsilon) \tag{2}$$

where $\omega = 2\pi f$. Amplitudes σ_0 and ε_0 and phases Φ_σ and Φ_ε were determined by least squares fitting of equations (1) and (2) to σ(t) and ε(t), respectively. Detailed equations used in this calculation are presented in Appendix A of the companion paper [*Takei et al.*, 2011]. Using the assumption of constant volume, a correction was applied to sample length and area to account for accumulated strain, the magnitude of which is provided in Table 1. Young's modulus E and inverse quality factor Q^{-1} are calculated by

$$\begin{cases} E = \dfrac{\sigma_0}{\varepsilon_0} \\ Q^{-1} = \tan\delta \end{cases} \tag{3}$$

where $\delta = \Phi_\varepsilon - \Phi_\sigma$ represents the phase lag of strain from stress. We further introduce the complex compliance $J^*(f)$ given by

$$J^*(f) = J_1(f) + iJ_2(f) = \frac{\varepsilon_0}{\sigma_0} e^{i\delta} \tag{4}$$

the real and imaginary parts of which are termed the "storage compliance" and "loss compliance," respectively, defined by

$$\begin{cases} J_1(f) = \dfrac{\varepsilon_0}{\sigma_0}\cos\delta = \dfrac{1}{E(f)\sqrt{1+(Q^{-1}(f))^2}} \\ J_2(f) = \dfrac{\varepsilon_0}{\sigma_0}\sin\delta = \dfrac{Q^{-1}(f)}{E(f)\sqrt{1+(Q^{-1}(f))^2}} \end{cases}. \tag{5}$$

[18] The present tests were performed under $\varepsilon = \varepsilon_{zz}$, $\sigma = \sigma_{zz}$ and $\sigma_{xx} = \sigma_{yy} = 0$. To emphasize these experimental conditions, Q^{-1} and J^* introduced above can be written as Q_E^{-1} and J_E^*, respectively, where subscript E represents Young's modulus. When Q^{-1} and J^* corresponding to bulk and shear moduli are written as Q_k^{-1}, Q_μ^{-1}, J_k^*, and J_μ^*, J_E^* is related to J_k^* and J_μ^* by $J_E^* = J_k^*/9 + J_\mu^*/3$. Therefore, $Q_E^{-1} = J_2^E/J_1^E$ is related to $Q_k^{-1} = J_2^k/J_1^k$ and $Q_\mu^{-1} = J_2^\mu/J_1^\mu$ as

$$Q_E^{-1} = \xi Q_k^{-1} + (1-\xi) Q_\mu^{-1} \tag{6}$$

where

$$\xi = \frac{J_1^k}{J_1^k + 3J_1^\mu}. \tag{7}$$

Factor ξ depends on the Poisson's ratio. Using the Poisson's ratio of borneol at ultrasonic frequency (0.37) [*Takei*, 2000], we obtain $\xi = 0.086$. Therefore Q_E^{-1} contains very little contribution from bulk attenuation and is a good approximation of Q_μ^{-1}.

2.4.2. Creep Tests

[19] With constant stress σ and strain rate $\dot{\varepsilon}$, steady state viscosity is calculated as $\eta = \sigma/\dot{\varepsilon}$. As in section 2.4.1, a correction was applied to the data to account for the change in sample length and area as a result of accumulated strain, the magnitude of which is provided in Table 1. Viscosity η can be described through a combined power law and Arrhenius equation of the form

$$\eta = \eta_0 \left(\frac{d}{d_r}\right)^m \exp\left[\frac{U}{R}\left(\frac{1}{T} - \frac{1}{T_r}\right)\right] \tag{8}$$

where d is grain size, m is the grain size exponent, U is the activation energy for creep, R is the gas constant, T is temperature, and subscript r refers to the reference grain size and temperature. Just as in section 2.4.1, η for this study can be written as η_E, and is related to shear viscosity η_μ as

$$\eta_E = 3\eta_\mu \tag{9}$$

where bulk viscosity η_k is assumed to be infinite.

2.5. Application of the Kramers-Kronig Relations

[20] Compliances J_1 and J_2 introduced in section 2.4.1 are related by the Kramers-Kronig relations as

$$\begin{cases} J_1(\omega) = J_U + \displaystyle\int_{\tau=0}^{\tau=\infty} X(\tau)\frac{1}{1+(\omega\tau)^2}\frac{d\tau}{\tau} \\ J_2(\omega) = \displaystyle\int_{\tau=0}^{\tau=\infty} X(\tau)\frac{\omega\tau}{1+(\omega\tau)^2}\frac{d\tau}{\tau} + \frac{1}{\omega\eta} \end{cases} \tag{10}$$

where J_U is the unrelaxed elastic compliance and $X(\tau)$ represents the so-called *relaxation spectrum* at time scale τ [*Nowick and Berry*, 1972, p. 78]. Parameter J_U is related to the unrelaxed Young's modulus E_U as $J_U = 1/E_U$. Because J_1 and J_2 are measured almost independently from amplitude ratio and phase delay, respectively, this theoretical relationship can be used to check the internal-consistency of the data. In previous studies, this relationship was used in limited form in the Andrade model and an extended Burgers model, which assume $X(\tau)$ as power law (τ^α) and box-car × power law functions, respectively, with a constant power α [e.g., *Tan et al.*, 2001; *Jackson et al.*, 2002; *Gribb and*

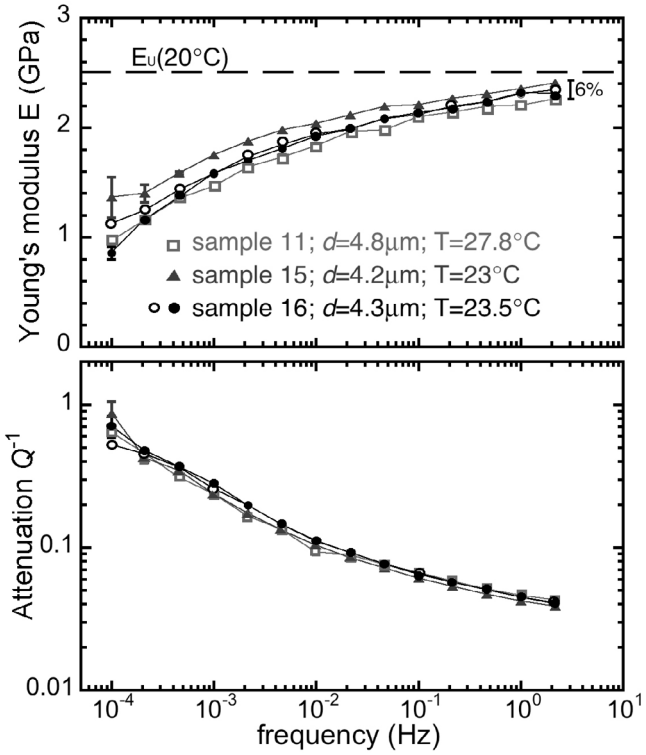

Figure 4. E and Q^{-1} for three borneol samples at nearly constant grain size and temperature. The multiple symbols for sample 16 correspond to tests conducted on successive days (closed symbol was first). Error bars correspond to the average and standard deviation of three separate calculations of E and δ using various windows of time.

Cooper, 1998]. In this study, we introduce an alternate method in which a functional form of $X(\tau)$ is not postulated a priori but is instead obtained directly from J_1 and J_2 data via the Kramers-Kronig relations. By assuming that X is a continuous function smoothly varying with respect to $\ln\tau$, the factors in equation (10) are well approximated by a step-function and a delta-function, as

$$\begin{cases} \dfrac{1}{1+(\omega\tau)^2} = H(-\ln\tau - \ln\omega) \\ \dfrac{\omega\tau}{1+(\omega\tau)^2} = \dfrac{\pi}{2}\delta(\ln\tau + \ln\omega) \end{cases} \tag{11}$$

such that

$$\begin{cases} J_1(p) = J_U + \displaystyle\int_{\tau=0}^{\tau=p/2\pi} X(\tau)\frac{d\tau}{\tau} \\ J_2(p) = \dfrac{\pi}{2}X\left(\tau = \dfrac{p}{2\pi}\right) + \dfrac{p}{2\pi\eta} \end{cases} \tag{12}$$

where $p = 1/f$ is period [*Nowick and Berry*, 1972]. From equation (12), J_1 and J_2 can be related by

$$J_1(p) + \frac{p-p_r}{\pi^2\eta} = J_1(p_r) + \frac{2}{\pi}\int_{p'=p_r}^{p'=p} J_2(p')\frac{dp'}{p'} \tag{13}$$

where $J_1(p_r)$ represents an initial value of J_1 for the integration of equation (13) at an arbitrarily taken reference period p_r. We apply equation (13) to measured J_1 and J_2 curves to check the internal-consistency of the data and to estimate η. Then, by substituting J_2 and η into the second equation of equation (12), we estimate $X(\tau)$. The only assumption made with our method, in addition to linearity, is that $X(\tau)$ is smooth. As shown in section 3.3, this method enables us to observe that the time scale dependence of $X(\tau)$ is not constant.

3. Experimental Results

3.1. Reproducibility and General Form

[21] Figure 4 shows experimental data for three samples with similar grain sizes (4.15–4.8 μm) and temperatures (23–27.8°C) evidencing the reproducibility of both modulus and attenuation data. As discussed in the companion paper, the discrepancy in the absolute value of E that is attributed to random error of the apparatus (likely due to meter sensitivity) is 5–6% over all frequencies. The discrepancy in E between similar samples (e.g., at $f = 2.15$ Hz in Figure 4) is consistent with this random error, the magnitude of which must therefore exceed any sample fabrication or assemblage error. Over the range of testing conditions, the modulus relaxes by ~60% of the published unrelaxed modulus.

[22] Although random error affects E, it does not affect Q^{-1}. The error in determination of Q^{-1} is primarily dependent on error in measuring the phase lag, which is very small. Consistently, Q^{-1} measurements are highly reproducible and extremely robust. Even the small discrepancy in Q^{-1} between samples 15 and 16 in Figure 4 is not attributed to scattering but rather can be supported by the small difference in the modulus dispersion. The error bars shown in Figure 4 represent the uncertainty produced by removal of linear trends from the data. As discussed in section 2.4.1, this error can be large at $f = 10^{-4}$ Hz but nearly zero for $f \geq 0.000464$. The general form of Q^{-1} is that of a moderate power law relationship with frequency that accelerates slightly at low frequency and flattens at high frequency. The coverage of the data set allows us to see a smooth function over more than four decades of frequency, with no visible Debye peaks.

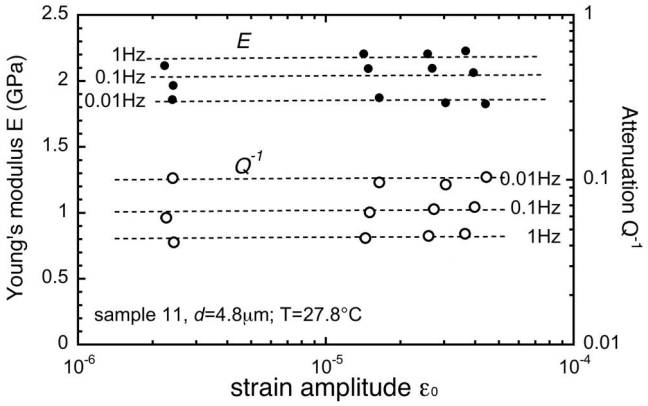

Figure 5. E and Q^{-1} versus strain amplitude at several fixed frequencies showing linearity of anelastic response independent of strain amplitude at the conditions of testing.

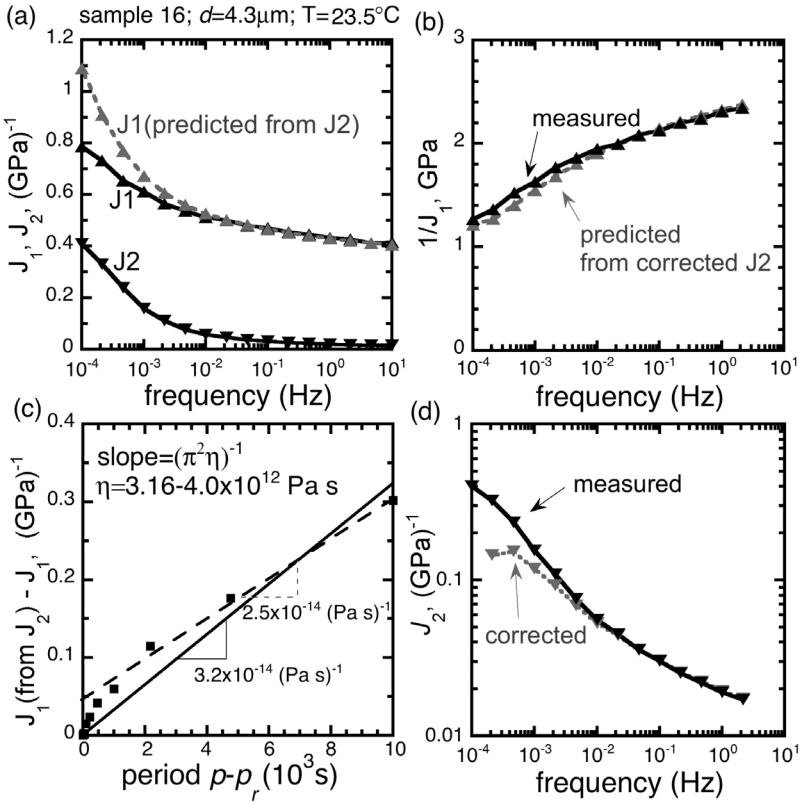

Figure 6. Application of the Kramers-Kronig (K-K) relations to anelasticity data. (a) "Measured" J_1 and J_2 obtained from the measured E and Q^{-1}, which are compared to the "predicted" J_1 calculated from measured J_2. (b) Measured J_1 compared to the predicted J_1 calculated from J_2 corrected for the viscosity term. Data are shown inversely to correspond to units of modulus. (c) The difference between the measured and predicted J_1, when plotted against period, provides viscosity. (d) Measured J_2 compared to J_2 corrected for the viscosity term.

3.2. Linearity of the Viscoelastic Response

[23] Figure 5 shows that, for a suite of tests conducted on sample 11 at constant grain size (d = 4.8 μm) and constant temperature (T = 27.8°C) for multiple stress/strain amplitudes ($\sigma_0 \cong$ 0.077, 0.055, 0.030, and 0.0045 MPa), the measured modulus and attenuation are independent of strain amplitude. In a separate study, steady state uniaxial creep experiments performed on a borneol aggregate under similar conditions to our creep experiments (d = 3.6 μm; T = 20°C; σ = 0.11–0.38 MPa) showed a stress exponent of nearly one [*Watanabe*, 2011]. Therefore, the mechanical linearity of the viscoelastic response can be deduced for all frequencies studied. The amplitude independence justifies our use of a single value of driving stress amplitude (σ_0 = 0.055 MPa) for the rest of this study. The linearity of the response also justifies application of the Kramers-Kronig relations to our data.

3.3. Application of the Kramers-Kronig Relations

[24] To analyze the quality of each data set, J_1 and J_2 curves were calculated using equation (5). Figure 6a displays representative curves from sample 16 at d = 4.3 μm and T = 23.5°C (black symbols). Both J_1 and J_2 increase monotonically with decreasing frequency. The right hand side of equation (13) is calculated based on the J_2 data and J_1 (p_r = 1 s) and is plotted in Figure 6a as the "predicted J1" (gray symbols). The difference between the two curves of J_1 is $(p - p_r)/\pi^2\eta$ and thus, when plotted against period $p - p_r$, viscosity η is estimated from the slope as η = 3.16–4.0 × 10^{12} Pa s (Figure 6c). We compare this viscosity obtained from the anelasticity data to the independently obtained viscosity measurements from creep tests ($\eta \cong 4.1 \times 10^{12}$ Pa s, Table 1, sample 16, d = 4.3 μm) and see good agreement between the two. Generally, η estimated from the anelasticity data has larger error than η determined from creep tests, especially when there is a large error bar in the data at the lowest frequency ($f = 10^{-4}$ Hz; Figure 4).

[25] In Figure 6d we compare J_2 obtained from directly measured E and Q^{-1} data (black) to J_2 after removal of the viscosity term $p/2\pi\eta$ (gray). The second equation of equation (12) shows that J_2 corrected for the viscosity term represents $(\pi/2)X(\tau = 1/2\pi f)$, the purely anelastic response. In Figure 6b, we compare the measured J_1 (black) to the predicted J_1 (gray), which was calculated using the corrected J_2. The good agreement between the two J_1 curves in Figure 6b confirms the consistency between the J_1 and J_2 data (or E and Q^{-1} data) with respect to the Kramers-Kronig relations.

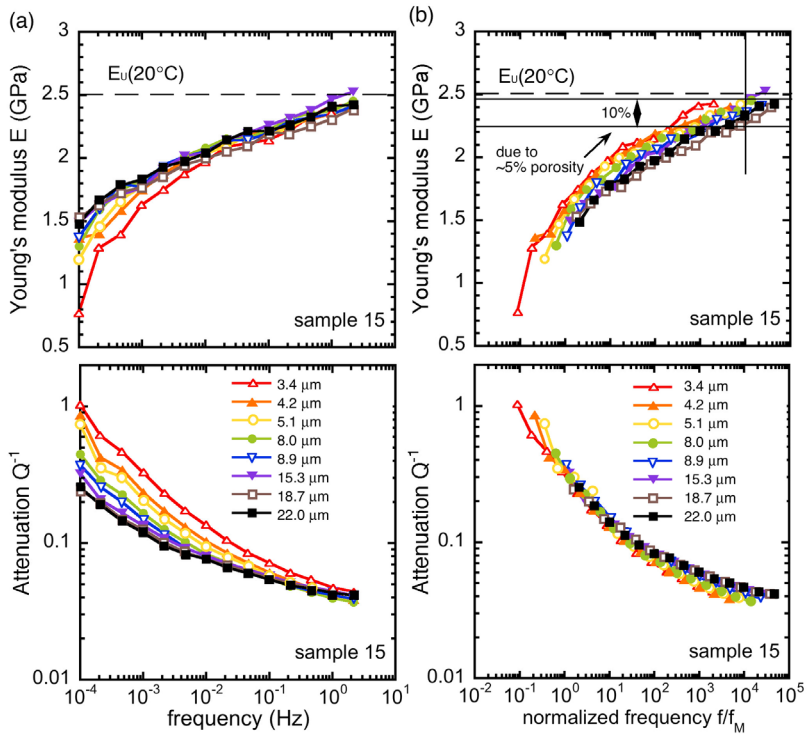

Figure 7. (a) Anelasticity data showing grain-size sensitivity of Young's modulus and attenuation for sample 15, under approximately constant temperature T = 22.4–23.6°C. The sample has been annealed for various durations (listed in Table 1) to achieve the grain sizes listed. (b) Same data from Figure 7a, as functions of frequency normalized by the Maxwell frequency.

[26] In the above mentioned method, the relaxation spectrum $X(\tau)$ can be estimated directly from the data without assuming any specific functional form (Figure 6d, gray symbols). After correction for the viscosity term, the power law relationship shows a nearly constant slope at low frequency. However, at higher frequencies the slope decreases considerably.

3.4. Grain Size Results

[27] Anelasticity data at various grain sizes (3.35–22 μm) and at approximately constant temperature (22.4–23.6°C) are shown in Figure 7a, which demonstrates the notable effect of grain size on the anelastic response of polycrystalline borneol (sample 15; see Table 1 for details). As grain size increases, modulus dispersion and attenuation generally decrease. However, the grain size sensitivity of modulus dispersion and attenuation is not constant over the entire range of frequencies tested; there is considerable grain size effect observed at low frequency with little to no effect at high frequency. Similar results were also obtained for sample 16, the data from which we provide in Appendix A to demonstrate the reproducibility of the grain size tests (Figure A1a).

[28] Figure 8 shows unidirectional (steady state) creep data at various grain sizes, (3.35–22 μm) and at approximately constant temperature (22.4–23.6°C). The results show that as grain size increases, steady state viscosities increase significantly. A logarithmic plot of viscosity versus grain size was calculated in which two distinct relationships can be observed (Figure 8b). At small grain size ($d < 7$ μm) a cubic relationship is shown (i.e., $m = 3$ in equation (8)), whereas at larger grain size, this grain size relationship decreases to a shallower slope. The cubic relationship is consistent with steady state creep that is rate-controlled by grain boundary diffusion. That the sample was deforming by grain boundary diffusion creep was also supported by a separate study in which a stress exponent of nearly one was obtained with this same material under similar experimental conditions [*Watanabe*, 2011].

3.5. Temperature Results

[29] Data for anelasticity at various temperatures in the range 23.7 to 45.4°C (T/T_m = 0.62–0.67) and at nearly constant grain size (22 μm) are shown for sample 15 in Figure 9a. As temperature increases, modulus dispersion and attenuation increase. Similar results were obtained for sample 17, the data from which we provide in Appendix A to demonstrate the reproducibility of the temperature tests (Figure A2a). Figure 10 shows unidirectional creep data at various temperatures and at constant grain size for sample 15. From the Arrhenius plot in Figure 10b, an activation energy (i.e., U in equation (8)) of ~85 kJ mol^{-1} was calculated.

3.6. Normalization Results

[30] In both grain size tests and temperature tests, strong correlation between anelasticity and viscosity was obtained; modulus dispersion and attenuation tend to increase with decreasing viscosity. Therefore, we normalized data from each

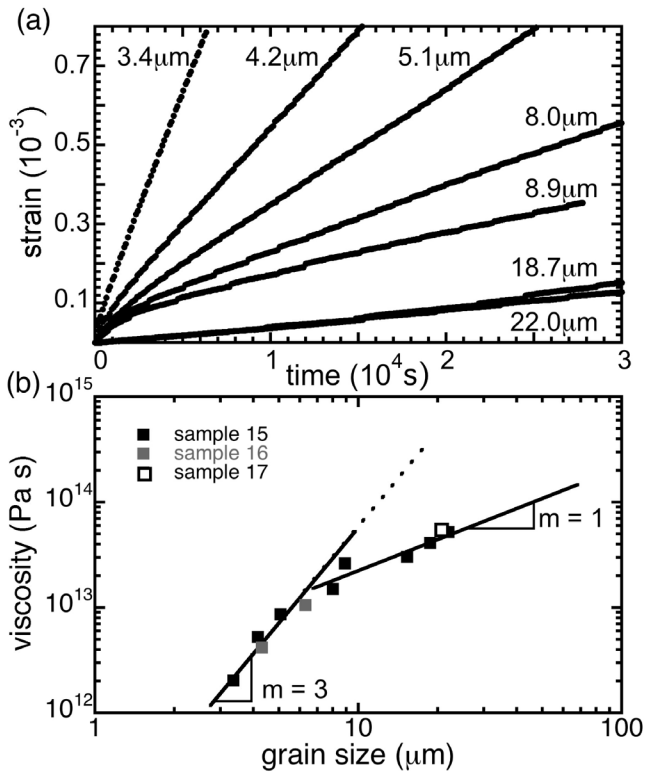

Figure 8. Unidirectional creep data showing the grain size sensitivity of (a) creep curves for sample 15 and (b) viscosity (samples 15, 16, and 17), at T = 22.4–23.6°C and in all cases under a quasi-static applied stress of 0.28 ± 0.01MPa.

grain size d and temperature T by the Maxwell relaxation frequency:

$$f_M(d,T) = \frac{E_U(T)}{\eta_E(d,T)} \tag{14}$$

determined from directly measured viscosities and the unrelaxed Young's modulus from ultrasonic measurements. The value of $\tau_M = 1/f_M$ used for each data set is provided in Table 1. In Figure 7b, E and Q^{-1} from grain size tests are plotted as functions of normalized frequency f/f_M, showing the collapse of curves to a single master curve. (The relatively large scatter in modulus data is discussed below.) In Figure 9b, E normalized to $E_U(T)$ and Q^{-1} from temperature tests on sample 15 are plotted as functions of normalized frequency f/f_M, again showing the collapse to a single master curve for each. A similar collapse of modulus and attenuation data for samples 16 and 17 is demonstrated in Figures A1b and A2b.

[31] Modulus data from grain size tests of sample 15 (Figure 7b, top) display considerable scatter. At fixed normalized frequency, the discrepancy is about 10%, with E tending to decrease with increasing grain size. This scatter can be attributed to the formation of porosity due to grain growth in the absence of confining pressure. Microstructural analysis of sample 15 after all mechanical tests were completed revealed an increase in porosity by several percent (Figure 11), which was found to be greater in the center of the sample and decreased radially. Miniature samples showed little to no porosity. That measured grain sizes of the inner (d = 21.4 μm) and outer (d = 21.6 μm) portions of the testing sample and the relatively pore-free miniature sample (d = 22 μm) were consistent confirms that porosity did not affect grain growth. Based on the effective medium theory, assuming spherical cavities [*Berryman*, 1995], a 10% decrease in Young's modulus is predicted with a porosity of 5%. As shown in Figure 11, this amount of porosity is roughly consistent with microscopic observation. Consequently, without a change in porosity, modulus data, too, are expected to collapse onto a single curve. This hypothesis is also supported by the perfect collapse of the modulus data from temperature tests (Figures 9b and A2b), which are considered to be at constant grain size (i.e., constant porosity). Scattering of attenuation spectra is much smaller than modulus data (Figure 7b), indicating that the effect of porosity on attenuation is small.

[32] Figure 12 shows normalized modulus $E/E_U(T)$ and attenuation Q^{-1} from both grain size tests and temperature tests as functions of normalized frequency for sample 15. All attenuation spectra collapse to a single master curve, demonstrating that both grain size and temperature effects can be captured by this simple Maxwell frequency scaling. The modulus data from temperature tests collapse onto the data from the larger grain sizes of the grain size tests, which again suggests that without porosity change, modulus data from both tests would collapse onto a single master curve.

4. Discussion

4.1. Similarity and Universality of Anelasticity

[33] The results of our study have demonstrated that both grain size and temperature effects on anelasticity are captured by the Maxwell frequency scaling. We found, too, that similitude in the anelastic response extends to samples with gross material differences. Figure 13 shows Q^{-1} spectra versus normalized frequency of various olivine-dominated aggregates measured in torsion [*Tan et al.*, 2001; *Jackson et al.*, 2002; *Gribb and Cooper*, 1998], in addition to those of organic aggregates from this study. Maxwell frequencies for the torsion experiments were calculated by $f_M = \mu_U/\eta_\mu$, using the following values: μ_U = 63 GPa for T = 1200°C [*Isaak*, 1992]; $\eta_\mu = 6.28 \times 10^{13}$ Pa s for d = 23.6 μm and T = 1200°C [*Tan et al.*, 2001, #6261]; $\eta_\mu = 0.72 \times 10^{13}$ Pa s for d = 2.9 μm and T = 1200°C [*Jackson et al.*, 2002, #6381]; and $1/f_M$ = 414/4 s and 59/4 s for $d \approx 3$ μm and T = 1200°C and 1250°C, respectively [*Gribb and Cooper*, 1998]. The consistency among the various normalized spectra is remarkable. The efficacy of this simple scaling demonstrates the true universality of the master curve to polycrystalline materials and also validates our use of borneol as an analogue to olivine in attenuation studies. Here, a direct comparison of modulus data was not performed because modulus data are generally subject to larger error than Q^{-1} data. However, in section 4.3, our modulus results are discussed in comparison with those of *Jackson et al.* [2002].

[34] These findings can be expressed as a "similarity rule." Whereas the Q^{-1} spectrum represents a mixed effect of anelastic relaxation, modulus dispersion, and viscous deformation, the relaxation spectrum $X(\tau)$ introduced in

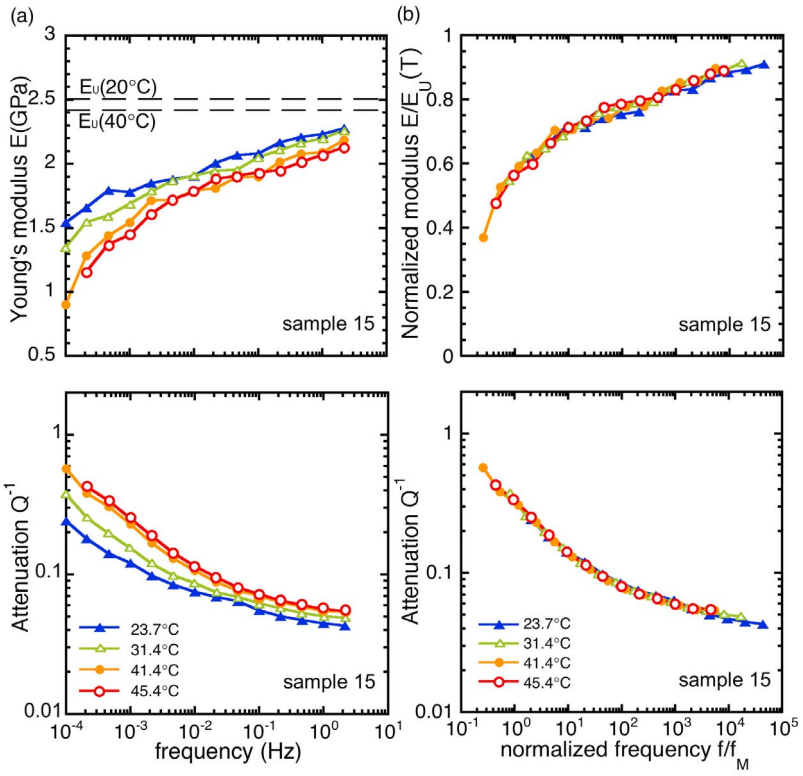

Figure 9. (a) Anelasticity data showing the temperature dependence of Young's modulus and attenuation for sample 15 with constant grain size (d = 22 μm). (b) Same data as in Figure 9a, as functions of frequency normalized to the Maxwell frequency.

section 2.5 represents the strength of a purely anelastic relaxation at time scale τ. Because modulus dispersion and viscous deformation are significant in experimental studies, the use of X to describe similarity rather than Q^{-1} greatly simplifies the formulation. We first introduce a normalized relaxation spectrum X_{n}, defined by

$$X_n = \frac{X}{J_U(T,P)} \tag{15}$$

so that the formulation is applicable to any P-T condition in the Earth. Unrelaxed compliance J_U is considered known as a function of T and P. Subscript n is used to denote normalized quantities. The similarity rule for anelasticity can be formulated such that the normalized relaxation spectrum X_{n}, which generally depends on time scale τ, grain size d, temperature T, and pressure P, is a unique function of the normalized time scale τ_{n}:

$$X_n(\tau, d, T, P) = X_n(\tau_n) \tag{16}$$

where τ_{n} is defined by using a reference time scale τ_{r} as

$$\tau_n(\tau, d, T, P) = \frac{\tau}{\tau_r(d, T, P)}. \tag{17}$$

The nature of the reference time scale τ_{r} dependence on d, T, and P provides valuable information about the mechanism causing the anelastic relaxation. We introduce τ_{r} independently from the Maxwell relaxation time scale τ_{M}, so that the present formulation is applicable to the studies of *Jackson et al.* [2002] and *Faul and Jackson* [2005], in which $\tau_{\mathrm{r}} \neq \tau_{\mathrm{M}}$.

[35] An important consequence of the similarity rule is a mutual relationship between the frequency, grain size, temperature, and pressure dependences of anelasticity: by substituting equations (16) and (17) into the Kramers-Kronig relations (equation (12)), we obtain

$$\begin{cases} J_1(f,d,T,P) = J_U(T,P)\left\{1 + \displaystyle\int_{\tau_n=0}^{\tau_n=(2\pi f_n)^{-1}} X_n(\tau_n)\frac{d\tau_n}{\tau_n}\right\} \\ J_2(f,d,T,P) = J_U(T,P)\left\{\dfrac{\pi}{2}X_n\left(\tau_n = \dfrac{1}{2\pi f_n}\right) + \dfrac{1}{2\pi f \tau_M}\right\} \end{cases} \tag{18}$$

where normalized frequency f_n is defined by

$$f_n(f,d,T,P) = f \cdot \tau_r(d,T,P). \tag{19}$$

By taking the partial derivative of measureable quantities J_1 and Q^{-1} ($= J_2/J_1$) with respect to each of f, d, T, and P, we obtain

$$\begin{cases} \left[\dfrac{\partial \ln J_1}{\partial \ln x}\right]_{y,z,w} = \left[\dfrac{\partial \ln J_U(T,P)}{\partial \ln x}\right]_{y,z,w} - \dfrac{2}{\pi}Q^{-1}\left[\dfrac{\partial \ln f_n}{\partial \ln x}\right]_{y,z,w} \\ \left[\dfrac{\partial \ln Q^{-1}}{\partial \ln x}\right]_{y,z,w} = -\left(\alpha - \dfrac{2}{\pi}Q^{-1}\right)\left[\dfrac{\partial \ln f_n}{\partial \ln x}\right]_{y,z,w} \end{cases} \tag{20}$$

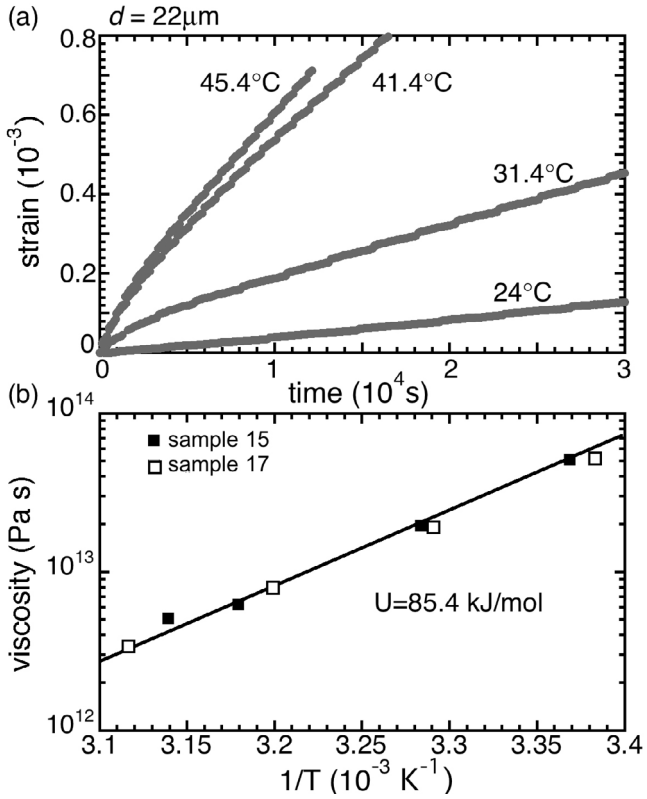

Figure 10. Unidirectional creep data showing the temperature sensitivity of (a) creep curves for sample 15 and (b) viscosity in samples 15 and 17 (Table 1).

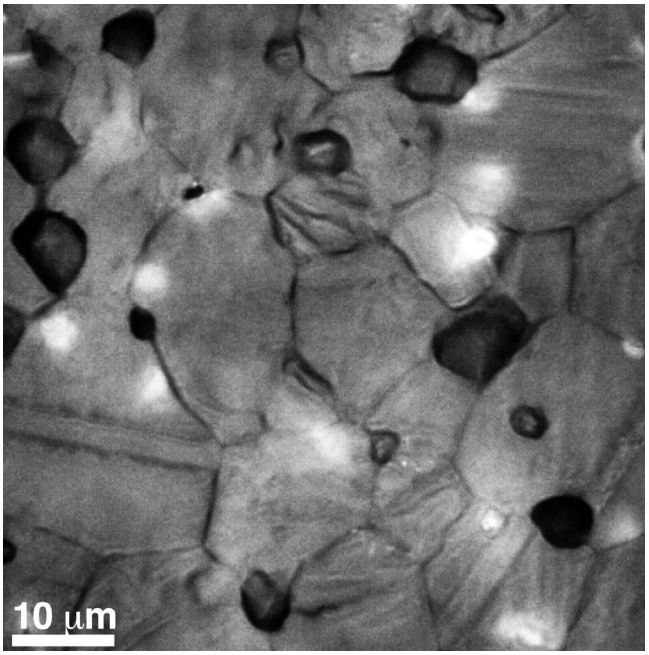

Figure 11. Light microscope image of borneol sample 15 post-deformation showing porosity (~6%) that has formed during the testing. Faint spots of light are interpreted as pores in the near subsurface. This image is from the center of the specimen. Porosity decreased with distance from the center.

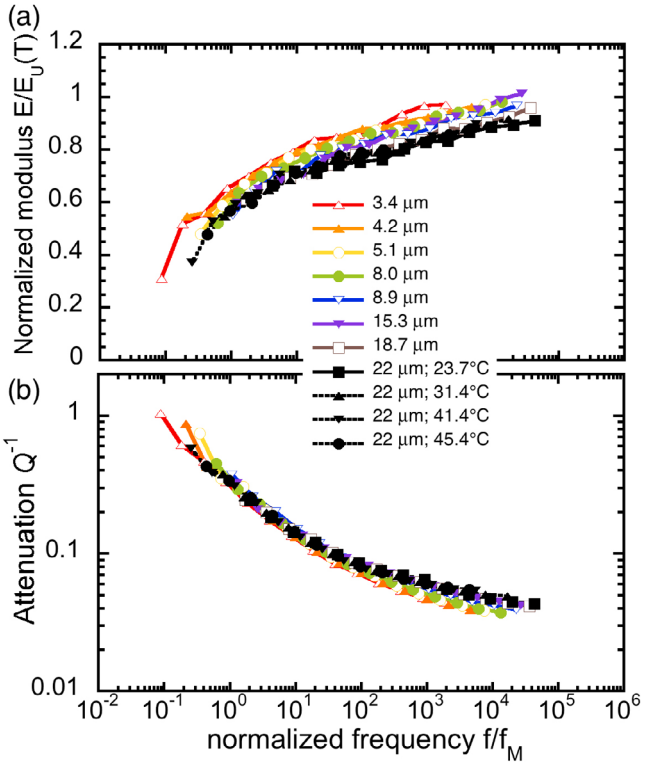

Figure 12. Normalized E and Q^{-1} data for all grain sizes and temperatures for sample 15, as functions of frequency normalized to the Maxwell frequency.

where parameter x for differentiation represents any one of the four variables f, d, T, and P, while the other three are shown by fixed variables y, z and w. Factor α is defined by

$$\alpha = \frac{d \ln X_n(\tau_n)}{d \ln \tau_n} \tag{21}$$

which represents the time scale exponent of the normalized relaxation spectrum or, in other words, the slope of the $\ln X_n$ versus $\ln \tau_n$ curve. In equation (20), the effect of viscous deformation on Q^{-1}, which is negligible at seismic frequency in the Earth, was neglected for simplicity.

[36] Once explicit functional forms of $\tau_r(d, T, P)$ and $X_n(\tau_n)$ are given, modulus and attenuation for any condition of f, d, T, and P can be calculated by equation (18) and the individual dependences of these can be calculated by equation (20). The explicit forms of $\tau_r(d, T, P)$ and $X_n(\tau_n)$ are provided in sections 4.2 and 4.3, respectively. The present formulation is general in that equations (15)–(21) can be used regardless of whether parameters X, J^*, Q^{-1}, η, and τ_M represent X_E, J^*_E Q_E^{-1}, η_E, and τ_M^E, respectively, or X_μ, J^*_μ Q_μ^{-1}, η_μ, and τ_M^μ, respectively, and so on.

4.2. Reference Time Scale and Underlying Mechanism

[37] Although similitude in the anelastic response of polycrystalline materials has been recognized in previous studies [*Gribb and Cooper*, 1998; *Jackson et al.*, 2002; *Morris and Jackson*, 2009a], determination of the appropriate reference time scale τ_r is still under debate. Characterization of the reference time scale is essential to identifying the underlying mechanism of anelasticity and

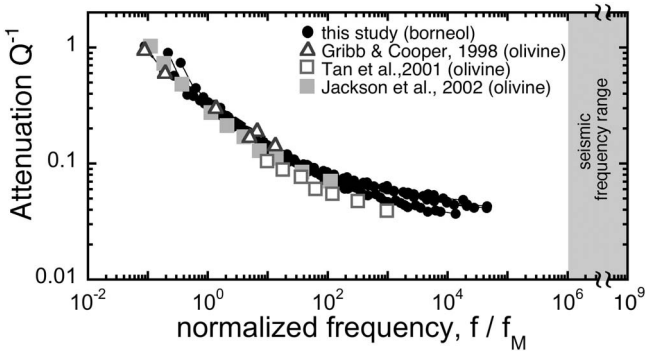

Figure 13. Measured Q^{-1} versus normalized frequency f/f_M from studies with gross material differences. For *Gribb and Cooper* [1998] T = 1200 and 1250°C; d = 3 μm. For *Tan et al.* [2001] T = 1200°C; d = 23.6 μm. For *Jackson et al.* [2002] T = 1200°C; d = 2.9 μm. These studies used olivine-dominated aggregates, whereas this study (black circles) used borneol aggregates at T = 22.4–45.4°C and d = 3.4–22 μm. The shaded area demonstrates that the normalized seismic frequency range is currently outside the range of experimental data.

also to extrapolating experimental data to a geophysical context. In this section we discuss the reference time scale, which we scrutinize for the operative mechanism of anelasticity. Implications for seismology are discussed in the next section.

[38] The experimental results of our study demonstrate that the reference time scale is a Maxwell time scale that is defined in terms of the steady state viscosity of diffusion creep (equation (8)):

$$\tau_r(d,T,P) = \tau_M(d,T,P) = J_U(T,P)\eta_0\left(\frac{d}{d_r}\right)^m \cdot \exp\left[\frac{U}{R}\left(\frac{1}{T}-\frac{1}{T_r}\right)\right]\exp\left[\frac{V}{R}\left(\frac{P}{T}-\frac{P_r}{T_r}\right)\right] \quad (22)$$

where the additional factor to equation (8) describes the pressure effect on viscosity with activation volume V and reference pressure P_r. Using equation (22), the unspecified factors in equation (20) are explicitly written as

$$\left[\frac{\partial \ln f_n}{\partial \ln x}\right]_{y,z,w} = \begin{cases} 1 & \text{for } x = f \\ m & \text{for } x = d \\ \left[\dfrac{\partial \ln J_U}{\partial \ln T}\right]_P - \dfrac{U+PV}{RT} & \text{for } x = T \\ \left[\dfrac{\partial \ln J_U}{\partial \ln P}\right]_T + \dfrac{PV}{RT} & \text{for } x = P \end{cases} . \quad (23)$$

That the anelastic relaxation follows the same scaling as steady state diffusion creep points to a physical process that is due to the same diffusional mechanism [e.g., *Raj*, 1975; *Gribb and Cooper*, 1998]. This requirement is met by "diffusionally accommodated grain boundary sliding," which explains well many other experimental observations. Grain boundary sliding ("GBS") is generally obstructed by grain edges and/or atomic-scale steps along the grain boundaries, causing local stress concentrations to build. With diffusionally accommodated GBS, relaxation of these stress singularities by diffusive matter transport through grain boundaries and/or grains is considered to be the rate-limiting step to sliding. Evolution of the stress state involving a wide range of diffusion path lengths from the atomic scale to the grain scale explains well the continuous and peakless shape of the relaxation spectrum [e.g., *Raj and Ashby*, 1971; *Morris and Jackson*, 2009b]. Additionally, the large modulus reduction (60%) observed in this study is consistent with this mechanism [e.g., *Zener*, 1941].

[39] As Figure 13 demonstrates, the attenuation data for olivine aggregates at various temperatures and grain sizes, from various source regions and various laboratories, collapse onto a single curve when normalized by the Maxwell relaxation frequency. In each study, the obtained activation energy was similar to that of diffusion creep. Thus, we propose that diffusionally accommodated GBS is operative in all of the studies shown in Figure 13. Any variations in the observed grain size dependences from one study to the next can be explained by equations (20) and (23). Specifically, the observation of approximately equal frequency and grain size exponents of Q^{-1} in the work of *Jackson et al.* [2002] is thoroughly consistent with equation (23) and their observed grain size exponent of viscosity of nearly one ($m \approx 1$).

[40] This interpretation deviates slightly from that of previous researchers. At higher frequencies (and/or lower temperatures), grain boundary sliding is accommodated not by diffusion but instead by local elastic deformation of grains. This elastically accommodated GBS is considered to be rate limited by "grain boundary viscosity." Although relatively well known in metal and ceramics, this process is poorly understood for rocks, and the relaxation strength and reference time scale τ_r are difficult to estimate. A simple elastic rebound model, for instance, predicts $\tau_r \propto d$. Based on such a model, the observation of approximately equal frequency and grain size dependences of Q^{-1} data in the work of *Jackson et al.* [2002] was attributed to elastically accommodated GBS [*Jackson et al.*, 2002; *Karato*, 2008]. As such, formulae with $\tau_r \neq \tau_M$ were used for the extrapolation of these data to mantle conditions [*Faul and Jackson*, 2005]. Contrary to this treatment, our experimental results show that the Maxwell frequency scaling is applicable for viscosities with a grain size exponent m = 3 (d < 7 μm), as well as for viscosities with a grain size exponent $m \approx 1$ (d > 7 μm), at all frequencies explored. Although m ≈ 1 is contrary to what one would expect for diffusion creep, the nearly identical spectra obtained for fine grained (m = 3) and coarse grained ($m \approx 1$) samples do not indicate a drastic difference in mechanisms between the two regimes. Further, we see no indication in our data of a Debye peak that is associated with elastically accommodated GBS in metals and ceramics. In our assessment, for all frequencies and grain sizes tested, the need to attribute spectra to a separate mechanism, which relies on a poorly constrained parameter of grain boundary viscosity, is unwarranted.

[41] Because elastically accommodated GBS occurs at higher frequencies than diffusionally accommodated GBS, there exists the possibility that the rate-limiting process of

relaxation changes at higher normalized frequencies than the experimental coverage. Indeed, attempts to detect such change have been performed [*Jackson and Faul*, 2010; *Sundberg and Cooper*, 2010]. In this study, the observation that the pore-free (d ~ 3.4 μm) modulus data approach E_U at high frequency (Figure 12) suggests that anelastic relaxation between ultrasonic and forced oscillation experiments is not strong. However, as discussed in section 4.3, this intermediate frequency range is important for seismological application and has to be assessed in more detail.

4.3. Application to Seismology

[42] Proving that the Maxwell frequency is the universal scaling factor for anelasticity allows for extrapolation of laboratory data to mantle conditions. In the upper mantle, the Maxwell frequency is estimated as 10^{11}Pa/10^{20}Pa s = 10^{-9} Hz. Therefore, the normalized frequency corresponding to the seismic frequency range (f = 1–10^{-3} Hz) is f/f_M = 10^6 – 10^9. Figure 13 shows that in normalized frequency space, experimental data cover a considerable range lower than, but do not include, the "seismic frequency range." Although previous experimental studies in the range f = 1–10^{-3} Hz have been considered to directly measure "seismic frequency," the much smaller grain sizes and much smaller viscosities of those experimental samples correspond to a significantly higher Maxwell frequency than that of mantle materials. To appropriately scale experimental data to seismology, it is important to measure anelasticity at higher frequencies, so that the detailed shape of the master curve can be revealed at $f/f_M = 10^6 - 10^9$. The extent to which the observed mechanism and scaling law are applicable at high normalized frequencies is not evident, and must be assessed as well. With typical laboratory viscosities in the range of 10^{12}–10^{13} Pa s, this corresponds to f = kHz, which is unfortunately between the current coverage of typical forced oscillation and ultrasonic (~MHz) tests, but is covered by a resonance method [*Lakes*, 1999]. Higher normalized frequencies can also be achieved at lower temperatures and/or larger grain sizes, though direct measurement of viscosity becomes difficult. More research, in the form of experiments and/or modeling, is needed.

[43] Nevertheless, strong efforts have been made to utilize laboratory measurements for interpreting regional and global seismological data [e.g., *Dalton et al.*, 2009; *Condor and Wiens*, 2006]. The studies primarily rely on the experimentally based model of *Faul and Jackson* [2005], which is particularly useful because it provides a generalized empirical formula for the frequency, grain size, and temperature dependences that allow extrapolation to upper-mantle conditions. Therefore we, too, generalize our present experimental results and extrapolate to mantle conditions. The findings of *Faul and Jackson* [2005] suggest that low-velocity and high Q^{-1} can be achieved by temperature variations alone. Because this model is being widely used in seismology, in particular to contest the need for partial melt, we feel it is important to carefully dissect the findings from that study and articulate the similarities and differences that we find with our results.

[44] Seismology is primarily concerned with relaxation of shear modulus μ, causing dispersion and attenuation of seismic shear waves. Shear wave velocity V_S and shear wave attenuation Q_S^{-1} can be directly calculated from J_1^μ and J_2^μ as

$$\begin{cases} V_S = \frac{1}{\sqrt{\rho J_1^\mu}} \\ Q_S^{-1} = \frac{J_2^\mu}{J_1^\mu} \end{cases} \quad \left(Q_S^{-1} \ll 1\right) \tag{24}$$

where ρ is density. (A more general form of equation (24), without the assumption of Q_S^{-1} « 1, is presented in Appendix B). When wave frequency f, grain size d, temperature T, and pressure P are given, J_1^μ and J_2^μ can be calculated from equation (18), in which explicit functional forms of τ_r (f, d, T, P) and $X_n(\tau_n)$ are needed. Here, we present these explicit forms by generalizing our experimental results. The explicit form of τ_r is given by equation (22), where d_r = 1 mm, m = 3, T_r = 1473 K, U = 505 kJ mol^{-1}, V = 1.2×10^{-5} m^3 mol^{-1}, and $\eta_0 = 6.6 \times 10^{19}$ Pa s. These parameters are selected such that the experimental conditions for grain size and viscosity can be continuously connected to upper mantle conditions. The unrelaxed shear modulus of olivine is $1/J_U^\mu(\mathrm{T, P}) = \mu_U(\mathrm{T, P}) = 82\ (\mathrm{GPa}) + 1.8 \times \mathrm{P(GPa)} - 0.0136\ (\mathrm{GPa/K}) \times \mathrm{T(K)}$ [*Isaak*, 1992]. The explicit form of $X_n(\tau_n)$ is obtained from curve fitting to the master curve which yields

$$X_n(\tau_n) = \begin{cases} 0.32 \times \tau_n^{0.39 - 0.28/\left(1 + 2.6 \times \tau_n^{0.1}\right)} & \tau_n \geq 10^{-11} \\ 1853 \times \tau_n^{0.5} & \tau_n < 10^{-11} \end{cases} \tag{25}$$

and is shown in Figure 14 as "fit1." (Because $Q_E^{-1} \cong 1Q_\mu^{-1}$ in this study, X_n obtained for E is comparable to X_n obtained for μ.) In the seismic range (shaded region), this curve agrees quite well with the value of $X_n^\mu(\sim 2\pi^{-1} Q_S^{-1})$ expected from seismological Q_S (= 80 in PREM; thick straight line) [*Dziewonski and Anderson*, 1981].

[45] For the ease of the reader, we provide a normalized J_1 curve that can be used to directly formulate V_S. The curve of J_1/J_U versus f_n calculated from X_n of "fit1" can be closely fit to a sixth-degree polynomial of ln f_n:

$$\frac{J_U(T,P)}{J_1(f,d,T,P)} = \begin{cases} \sum_{k=0}^{k=6} a_k (\ln f_n)^k & f_n \leq 10^{13} \\ 1 & f_n > 10^{13} \end{cases} \tag{26}$$

with a_0 = 0.55097, a_1 = 0.054332, a_2 = −0.0023615, a_3 = -5.7175×10^{-5}, $a_4 = 9.9473 \times 10^{-6}$, $a_5 = -3.4761 \times 10^{-7}$, and $a_6 = 3.9461 \times 10^{-9}$. This polynomial has perfect agreement with the original curve shown in Figure 15. Therefore, when f, d, T, and P are given, by substituting f_n calculated from equations (19) and (22) into equation (26), and also by using a known value of $J_U(T,P)$, J_1 (and therefore V_S) can be estimated easily. Also, by calculating J_2 from equations (18) and (25), Q_S^{-1} can be estimated. Finally, by substituting Q_S^{-1} into equation (20), partial derivatives can be estimated as well. Now, we have provided all information required to predict V_S and Q_S^{-1} as functions of f, d, T, and P. Before applying these predictions to the mantle, we compare the formulae with those of *Faul and Jackson* [2005], and also to our experimental data.

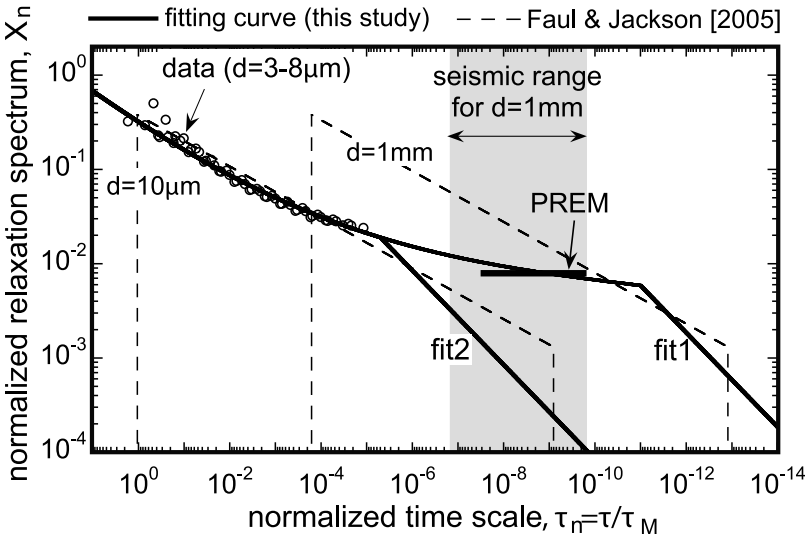

Figure 14. Normalized relaxation spectrum X_n obtained from our data is extrapolated toward shorter time scales by curve fitting. Fit1 corresponds to the large grain size in the mantle and fit2 corresponds to the fine grain size in the experiment (see text for more detail). Fit1 predicts a relaxation consistent to that of seismic observations, labeled PREM. For comparison, X_n by *Faul and Jackson* [2005] is shown (dashed lines). In this study, X_n is a unique function of the time scale normalized by the Maxwell relaxation time τ_M. In the work of *Faul and Jackson* [2005], X_n has a different reference time scale than τ_M and explicitly depends on grain size in this plot by τ/τ_M.

[46] In *Faul and Jackson* [2005], the grain size exponent of τ_r is nearly one (1.09) and is different from that of τ_M. As a consequence, when scaled by τ_M, the X_n proposed by *Faul and Jackson* [2005] is no longer a unique function of normalized time scale, but explicitly depends on grain size. Figure 14 demonstrates that relaxation strength X_n at the seismic range (shaded range) is considerably smaller in this study than it is in *Faul and Jackson* [2005] for d = 1 mm, whereas both are very close under the experimental condition (d = 10 μm). In other words, in this study the difference between laboratory attenuation and seismic wave attenuation comes from the difference in viscosity by about 10^6, whereas in *Faul and Jackson* [2005] it comes from the difference in grain size by about $10^{2\times1.09}$. While α (equation (21)) depends on τ_n in our study, α is a constant (0.27) in *Faul and Jackson* [2005]. In summary, the largest difference between the two studies is in τ_r and α.

[47] In order to compare the proposed extrapolation of X_n to our own experimental data, we substitute equation (25) into equation (18) to calculate predicted J_1/J_U and J_2/J_U as functions of f_n (Figure 15; solid lines), which we compare to our experimental data for d = 8 μm (Figure 15; symbols). Since J_1 represents the integration of $X_n(\tau_n)$ from τ_n = 0, it contains short time scale information of $X_n(\tau_n)$ that is outside the experimental range. Figure 15 shows that although predicted and measured J_2/J_U agree well, predicted J_1/J_U is systematically larger than measured J_1/J_U. If we reverse our methodology and instead look for an extrapolation of X_n that has good agreement to the measured J_1/J_U, such a spectrum is shown in Figure 14 as "fit2." The only difference between fit1 and fit2 is the time scale at which the relaxation spectrum transitions to $\tau_n^{0.5}$, which we call the "short-time-scale cut-off." In fit1, the cut-off occurs at $\tau_n = 10^{-11}$, while in fit2 it is at $\tau_n = 5 \times 10^{-6}$. Justification for cut-off times comes from a separate study, in which a theoretical model to describe the physics of diffusionally accommodated grain boundary sliding was developed [*Takei and McCarthy*, 2010]. In that model, GBS is obstructed by grain edges and atomic-scale steps along grain boundaries such that the cut-off time scale is determined by the size of each grain boundary step. The cut-offs in the mantle (fit1) and in the

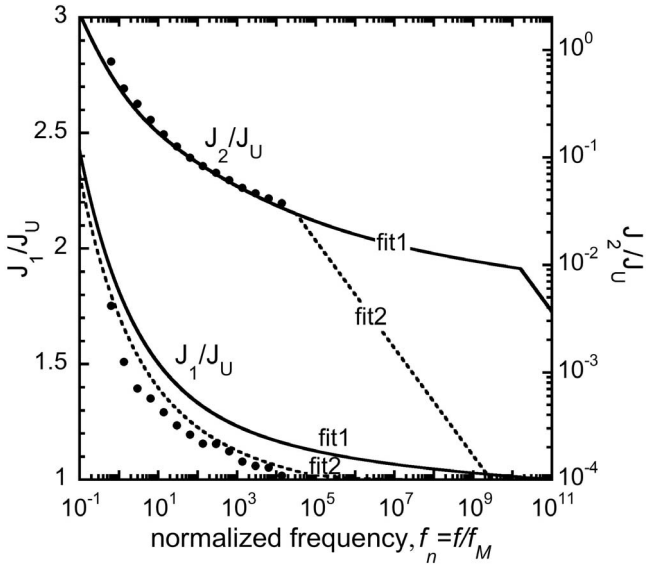

Figure 15. Plot of normalized frequency versus normalized J_1 and J_2 that were calculated using equation (18) and $X_n(\tau_n)$ given by fit1 and fit2 in Figure 14. Symbols show our data (d = 8 μm).

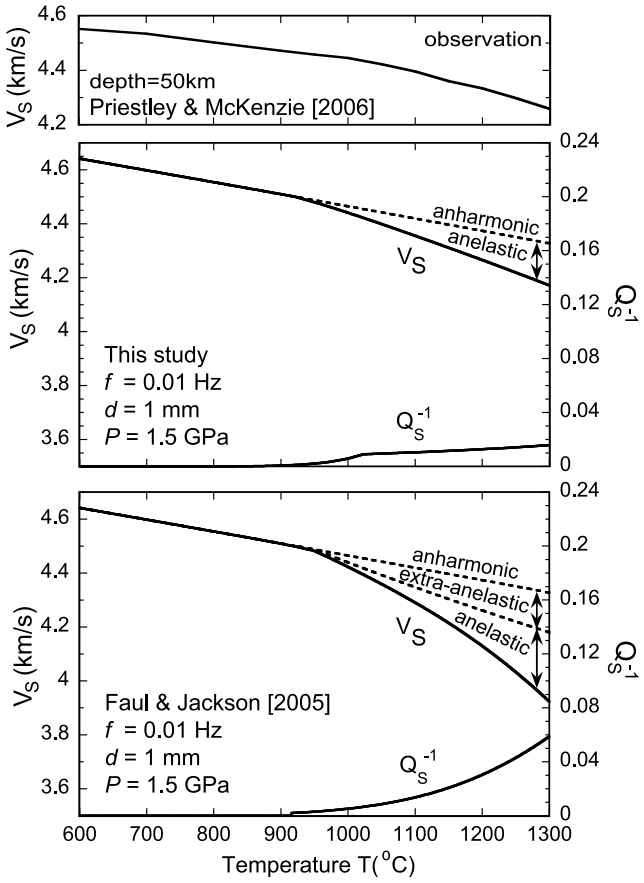

Figure 16. Schematic demonstrating the differences in temperature dependences of shear wave velocity and seismic attenuation between this study and *Faul and Jackson* [2005]. The temperature sensitivities of both V_S and Q_S^{-1} in the latter study are significantly greater than in our study.

experimental sample (fit2) are consistent with the preliminary result of this model that the cut-off time scale is about 100 Hz for a step size of about 10 nm. That fit2 has a considerably narrower band width than fit1 is a consequence of the fine grain size of experimental samples being closer to the step size (10 nm).

[48] Figure 16 shows the temperature dependences of V_S and Q_S^{-1} for f = 0.01 Hz, d = 1 mm and P = 1.5 GPa predicted by this study (Figure 16, middle) and *Faul and Jackson* [2005] (Figure 16, bottom). Because this study predicts smaller X_n (Figure 14), the predicted Q_S^{-1} and anelastic effect on V_S are significantly smaller than those of *Faul and Jackson* [2005]. Compared to the seismologically observed V_S (Figure 16, top) [*Priestley and McKenzie*, 2006], the predicted temperature dependence of V_S is slightly larger even at T < 900°C, where the slope is determined by the anharmonic effect alone. However, the steepening of the slope at about 1050°C observed in the seismological data can be explained fairly well by the deviation from the anharmonic effect due to the anelastic effect predicted by this study. As demonstrated in Figure 16, the results of *Faul and Jackson* [2005] have an "extra anelastic effect" which does not exist in our results. Unlike our data, modulus data of *Jackson et al.* [2002] were found to have a temperature dependence that could not be reconciled with simple anharmonic temperature sensitivity; with normalization their modulus data do not collapse onto a single master curve. Thus, their model incorporates an adjustment term. Such a finding implies that similitude for anelasticity breaks down at higher frequencies than 1 Hz in their study. Recently, however, *Jackson and Faul* [2010] showed that new data collected after an improvement was made to their experimental system could be analyzed without this extra effect. Therefore, we can state that so far no experimental data have clearly indicated a break down of similitude. Even without any experimental data, however, similitude for anelasticity has long been assumed in seismology [e.g., *Anderson and Given*, 1982]. With similitude, as shown by equation (20), only anharmonic and anelastic effects exist, both of which can be evaluated accurately from experimentally measured unrelaxed modulus and seismologically measured Q^{-1}, respectively [e.g., *Karato*, 1993].

5. Future Directions

[49] The results from this study demonstrate the universal behavior of polycrystalline materials in response to a periodic load in which the offset stress and periodic stress amplitude were small enough that the sample behaved linearly in both viscosity and anelasticity. By keeping stresses small we ensured a minimal amount of dislocations were created during the experiment and thus the observed response was due primarily to the diffusionally accommodated grain boundary sliding mechanism discussed herein. Not included in our experiment, or in our discussion, is relaxation due to dislocations, the contribution from which is considered to be *in addition* to the relaxation at grain boundaries. Characterization of that mechanism remains for future studies.

[50] The role of partial melt in dissipation and dispersion was also omitted from this study but represents a goal of our ongoing research. Experiments have already commenced in which we take advantage of eutectic phase relationships in the binary system borneol-diphenylamine [*Takei*, 2000] to obtain partial melt at temperatures as low as 43°C.

6. Conclusions

[51] Using a custom fabricated forced oscillation apparatus, linear anelasticity of an organic analogue material at high homologous temperature (T/T_m = 0.61–0.67) was measured accurately over a wide frequency range (2.15–10^{-4} Hz). Systematic effects of temperature and grain size on anelasticity were investigated, together with these effects on the steady state viscosity. At least for fine grain samples ($d < 7\mu$m), the creep mechanism could be identified as grain-boundary diffusion creep (m = 3). Using the directly measured viscosity, the Maxwell frequency was calculated as a function of temperature and grain size. Once frequency is normalized by the Maxwell frequency, modulus dispersion curves and attenuation spectra for various grain sizes and temperatures collapse onto a single master curve (similitude). With this simple scaling, attenuation spectra of olivine-dominated aggregates collapse onto the same master curve, showing a universality of anelasticity for polycrystalline materials. A new method to estimate the detailed shape of the relaxation spectrum $X(\tau)$ directly from modulus

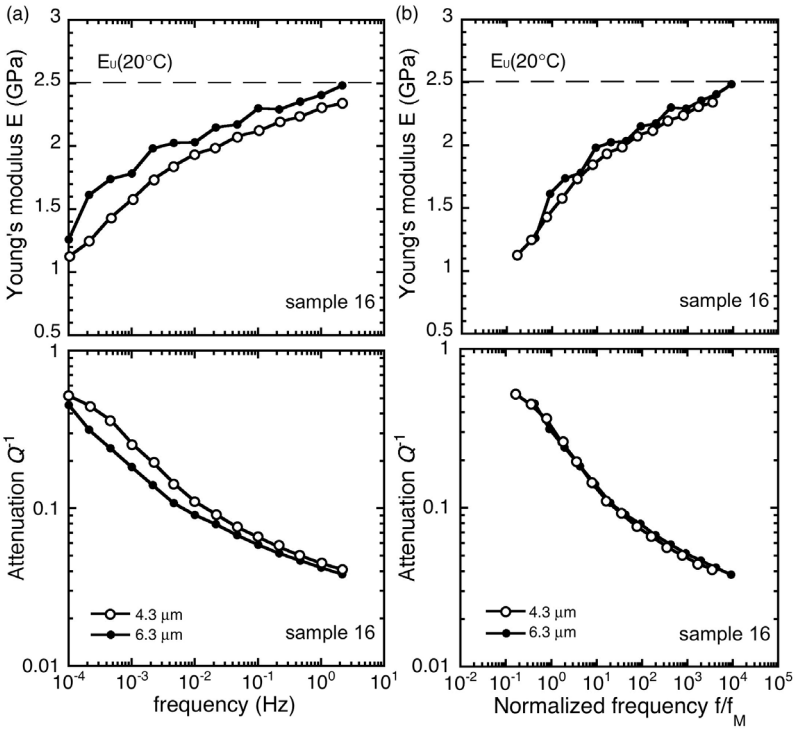

Figure A1. (a) Anelasticity data showing grain-size sensitivity of Young's modulus and attenuation for sample 16 under approximately constant temperature T = 23–23.5°C. The sample has been annealed (listed in Table 1) to achieve the grain sizes listed. (b) Same data from Figure A1a, as functions of frequency normalized to the Maxwell frequency.

and attenuation data was proposed by assuming smoothness of $X(\tau)$, whereas previous data analyses using Burgers model and Andrade model assume $X \sim \tau^{\alpha}$ with constant α. Our results show that α is not constant, but instead gradually decreases with decreasing time scale τ. The efficacy of the Maxwell frequency scaling, a continuous and peakless shape of the attenuation spectrum, and the large modulus reduction suggest that the dominant mechanism for the measured anelasticity is diffusionally accommodated grain boundary sliding. We generalize the obtained similitude and extrapolate the experimental data to mantle conditions. This Maxwell frequency scaling predicts a considerably smaller anelastic effect on seismic waves than in previous studies.

Appendix A: Reproducibility of Findings

[52] In Figures 7 and 9 we show results from grain size and temperature tests, respectively, on a single polycrystalline sample (15 in Table 1). In order to test the veracity of these results, we repeated experiments at various grain sizes and temperatures for two additional samples (16 and 17). Here, we provide Figure A1 to demonstrate the reproducibility of the grain size results. The anealasticity of sample 16 was measured at two grain sizes (4.5 and 6.2 μm) and at approximately constant temperature (23–23.5°C). Normalization by the Maxwell frequency resulted in good convergence of modulus data (very little scatter or porosity effects) and a near perfect collapse of attenuation data.

[53] In Figure A2, the reproducibility of temperature results is evidenced by the anelasticity data of sample 17 at various temperatures in the range 22.5–47.7°C (T/T_m = 0.61–0.67) and at nearly constant grain size (21.4 μm). As in Figure 9, the normalized modulus and attenuation data from temperature tests collapse onto single master curves.

Appendix B: Relationship Between Elastic Wave Properties and Material Properties

[54] In order to relate shear wave velocity V_S and shear wave attenuation Q_S^{-1}, we solve for the propagation of a plane wave in a linear solid. For simplicity, we consider a shear wave propagating in the x direction being polarized in the y direction. Then, the equation of the wave is given by

$$\rho \ddot{u}_y = \mu \frac{\partial^2 u_y}{\partial x^2} \tag{B1}$$

where μ represents the shear modulus and ρ represents the density. By considering a wave with angular frequency ω and wave number k, u_y can be written as

$$u_y = u_y^0 \exp(-i(\omega t - kx)). \tag{B2}$$

Expressing μ as $1/J^*(\omega)$ in the frequency domain, we obtain

$$\left(\frac{\omega}{k}\right)^2 = \rho J^*(\omega). \tag{B3}$$

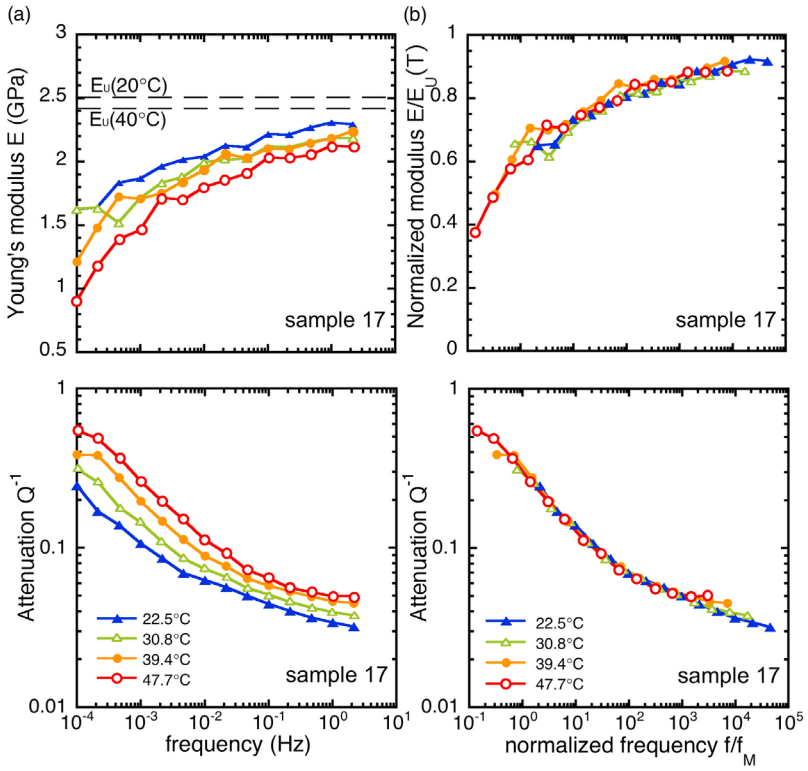

Figure A2. (a) Anelasticity data showing the temperature dependence of Young's modulus and attenuation for sample 17 with constant grain size ($d = 21.4$ μm). (b) Same data as in Figure A2a, as functions of frequency normalized to the Maxwell frequency.

Solving equation (B3), we obtain

$$u_y = u_y^0 \exp\left[-\omega x J_2 \left(\frac{\rho}{2(J_1 + \sqrt{J_1^2 + J_2^2})}\right)^{\frac{1}{2}}\right] \cdot \exp\left[-i\omega\left(t - \rho^{\frac{1}{2}}\left(\frac{J_1 + \sqrt{J_1^2 + J_2^2}}{2}\right)^{\frac{1}{2}} x\right)\right]. \quad \text{(B4)}$$

[55] Phase velocity V_S and quality factor Q_S of waves are defined as [e.g., *Aki and Richards*, 1980]

$$u_y = u_y^0 \exp\left[-\frac{\omega x}{2VQ_S}\right] \exp\left[-i\omega\left(t - \frac{x}{V}\right)\right]. \quad \text{(B5)}$$

By comparing equations (B4) and (B5), V_S and Q_S^{-1} are given by

$$\begin{cases} V_S = (\rho J_1)^{-\frac{1}{2}} \left(\dfrac{1 + \sqrt{1 + (J_2/J_1)^2}}{2}\right)^{-\frac{1}{2}} \\ Q_S^{-1} = \dfrac{J_2}{J_1}\left(\dfrac{1 + \sqrt{1 + (J_2/J_1)^2}}{2}\right)^{-1} \end{cases}. \quad \text{(B6)}$$

[56] Therefore, when $Q_S^{-1} \ll 1$ (or $J_2/J_1 \ll 1$), we obtain equation (24). Note that when Q_S^{-1} is not small, $Q_S^{-1} \neq Q_\mu^{-1}$.

[57] **Acknowledgments.** We thank M. Uchida at the Earthquake Research Institute for technical assistance and A. Yasuda for allowing us to access the microscope. We also thank S. Karato, R. Cooper, and F. Fusseis for helpful discussions and advice and I. Jackson and an anonymous reviewer for thoughtful and instructive reviews of this manuscript. This research was supported by the JSPS through grants 20340117, 21109005, and 22000003 and by the International office of the Earthquake Research Institute.

References

Aki, K., and P. G. Richards (1980), *Quantitative Seismology*, W. H. Freeman, San Francisco, Calif.

Anderson, D. L (1989), *Theory of the Earth*, Blackwell Sci., Boston.

Anderson, D. L., and J. W. Given (1982), Absorption band Q model for the Earth, *J. Geophys. Res.*, *87*(B5), 3893–3904, doi:10.1029/JB087iB05p03893.

Berryman, J. G. (1995), Mixture theories for rock properties, in *Rock Physics and Phase Relations: A Handbook of Physical Constants*, edited by T. J. Ahrens, pp. 205–228, AGU, Washington, D. C.

Condor, J. A., and D. A. Wiens (2006), Seismic structure beneath the Tonga arc and Lau back-arc basin determined from join Vp, Vp/Vs tomography, *Geochem. Geophys. Geosyst.*, *7*, Q03018, doi:10.1029/2005GC001113.

Dalton, C. A., G. Ekström, and A. M. Dziewonski (2009), Global seismological shear velocisty and attenuation: A comparison with experimental observations, *Earth Planet. Sci. Lett.*, *284*, 65–75, doi:10.1016/j.epsl.2009.04.009.

Duffy, T. S., and D. L. Anderson (1989), Seismic velocities in mantle minerals and the mineralogy of the upper mantle, *J. Geophys. Res.*, *94*, 1895–1912, doi:10.1029/JB094iB02p01895.

Dziewonski, A. M., and D. L. Anderson (1981), Preliminary reference Earth model, *Phys. Earth Planet. Inter.*, *25*, 297–356, doi:10.1016/0031-9201(81)90046-7.

Faul, U. H., and I. Jackson (2005), The seismological signature of temperature and grain size variations in the upper mantle, *Earth Planet. Sci. Lett.*, *234*, 119–134.

Gifkins, R. C. (1970), *Optical Microscopy of Metals*, Elsevier, New York.

Gribb, T. T., and R. F. Cooper (1998), Low-frequency shear attenuation in polycrystalline olivine: Grain boundary diffusion and physical significance of the Andrade model for viscoelastic rheology, *J. Geophys. Res.*, *103*, 27,267–27,279, doi:10.1029/98JB02786.

Isaak, D. G. (1992), High temperature elasticity of iron-bearing olivines, *J. Geophys. Res.*, *97*, 1871–1885, doi:10.1029/91JB02675.

Jackson, I., and U. H. Faul (2010), Grainsize-sensitive viscoelastic relaxation in olivine: Towards a robust laboratory-based model for seismological application, *Phys. Earth Planet. Inter.*, *183*, 151–163, doi:10.1016/j.pepi.2010.09.005.

Jackson, I., J. D. Fitz Gerald, U. H. Faul, and B. H. Tan (2002), Grain-size-sensitive wave attenuation in polycrystalline olivine, *J. Geophys. Res.*, *107*(B12), 2360, doi:10.1029/2001JB001225.

Jackson, I., U. H. Faul, J. D. Fitz Gerald, and B. H. Tan (2004), Shear wave attenuation and dispersion in melt-bearing olivine polycrystals: 1. Specimen fabrication and mechanical testing, *J. Geophys. Res.*, *109*, B06201, doi:10.1029/2003JB002406.

Jacobsen, S. D., F. Jiang, Z. Mao, T. S. Duffy, J. R. Smyth, C. M. Holl, and D. J. Frost (2008) Effects of hydration on the elastic properties of olivine, *Geophys. Res. Lett.*, *35*, L14303, doi:10.1029/2008GL034398.

Karato, S. (1993), Importance of anelasticity in the interpretation of seismic tomography, *Geophys. Res. Lett.*, *20*, 1623–1626, doi:10.1029/93GL01767.

Karato, S. (2008), *Deformation of Earth Materials: An Introduction to the Rheology of Solid Earth*, Cambridge Univ. Press, New York.

Karato, S., and H. Jung (1998), Water, partial melting and the origin of seismic low velocity and high attenuation zone in the upper mantle, *Earth Planet. Sci. Lett.*, *157*, 193–207, doi:10.1016/S0012-821X(98)00034-X.

Lakes, R. S. (1999), *Viscoelastic Solids*, CRC Press, Boca Raton, Fla.

Morris, S. J. S., and I. Jackson (2009a), Implications of the similarity principle relating creep and attenuation in finely grained solids, *Mater. Sci. Eng. A*, *521–522*, 124–127, doi:10.1016/j.msea.2008.09.157.

Morris, S. J. S., and I. Jackson (2009b), Diffusionally assisted grain-boundary sliding and viscoelasticity of polycrystals, *J. Mech. Phys. Solids*, *57*, 744–761, doi:10.1016/j.jmps.2008.12.006.

Nakajima, J., and A. Hasegawa (2003), Tomographic imaging of seismic velocity structure in and around the Onikobe volcanic area, northeastern Japan: Implications for fluid distribution, *J. Volcanol. Geotherm. Res.*, *127*, 1–18, doi:10.1016/S0377-0273(03)00155-0.

Nowick, A. S., and B. S. Berry (1972), *Anelastic Relaxation in Crystalline Solids*, Academic, San Diego, Calif.

Priestley, K. F., and D. P. McKenzie (2006), The thermal structure of the lithosphere from shear wave velocities, *Earth Planet. Sci. Lett.*, *244*, 285–301, doi:10.1016/j.epsl.2006.01.008.

Raj, R. (1975), Transient behavior of diffusion-induced creep and creep rupture, *Metall. Trans.*, *6A*, 1499–1509.

Raj, R., and M. F. Ashby (1971), On grain boundary sliding and diffusional creep, *Metall. Trans.*, *2*, 1113–1127, doi:10.1007/BF02664244.

Sherwood, J. N. (1979), Lattice defects, self-diffusion, and the plasticity of plastic crystals, in *The Plastically Crystalline State*, edited by J. N. Sherwood, pp. 39–83, Wiley Intersci., New York.

Stixrude, L., and C. Lithgow-Bertelloni (2005), Thermodynamics of mantle minerals-I. Physical properties, *Geophys. J. Int.*, *162*, 610–632, doi:10.1111/j.1365-246X.2005.02642.x.

Sundberg, M., and R. F. Cooper (2010), A composite viscoelastic model for incorporating grain boundary sliding and transient diffusion creep; correlating creep and attenuation responses for materials with a fine grain size, *Philos. Mag.*, *90*(20), 2817–2840, doi:10.1080/14786431003746656.

Takei, Y. (2000), Acoustic properties of partially molten media studied on a simple binary system with a controllable dihedral angle, *J. Geophys. Res.*, *105*, 16,665–16,682, doi:10.1029/2000JB900124.

Takei, Y., and C. McCarthy (2010) A granular model for anelasticity due to grain boundary sliding, Abstract MR11A–1864 presented at 2010 Fall Meeting, AGU, San Francisco, Calif., 13–17 Dec.

Takei, Y., K. Fujisawa, and C. McCarthy (2011), Experimental study of attenuation and dispersion over a broad frequency range: 1. The apparatus, *J. Geophys. Res.*, doi:10.1029/2011JB008382, in press.

Tan, B. H., I. Jackson, and J. D. Fitz Gerald (2001), High-temperature viscoelasticity of fine-grained polycrystalline olivine, *Phys. Chem. Miner.*, *28*, 641–664, doi:10.1007/s002690100189.

Tsumura, N., S. Matsumoto, S. Horiuchi, and A. Hasegawa (2000), Three-dimensional attenuation structure beneath the northeastern Japan arc estimated from spectra of small earthquakes, *Tectonophysics*, *319*(4), 241–260, doi:10.1016/S0040-1951(99)00297-8.

Watanabe, S. (2011), Experimental study of bulk and shear viscosities of partially molten analogue (in Japanese), Masters thesis, Univ. of Tokyo, Tokyo.

Wiens, D. A., K. Kelley, and T. Plank (2006), Mantle temperature variations beneath back-arc spreading centers inferred from seismology, petrology, and bathymetry, *Earth Planet. Sci. Lett.*, *248*, 30–42, doi:10.1016/j.epsl.2006.04.011.

Zener, C. (1941), Theoy of elasticity of polycrystals with viscous grain boundaries, *Phys. Rev.*, *60*, 906–908, doi:10.1103/PhysRev.60.906.

T. Hiraga, C. McCarthy, and Y. Takei, Earthquake Research Institute, University of Tokyo, 1-1-1 Yayoi, Bunkyo-ku, Tokyo, Japan. (mccarthy.christine@gmail.com)